Ab initio study of the structural phase transitions of the double perovskites Sr_2MWO_6 (M=Zn, Ca, Mg)

U. Petralanda and I. Etxebarria*

Fisika Aplikatua II Saila, Zientzia eta Teknologia Fakultatea, Euskal Herriko Unibertsitatea, P.K. 644, 48080 Bilbao, Spain

(Received 10 October 2013; revised manuscript received 17 January 2014; published 19 February 2014)

We study the interplay of structural distortions in double perovskites Sr_2MWO_6 (M = Zn, Ca, Mg) by means of first-principles calculations and group theoretical analysis. Structure relaxations of the cubic, tetragonal, and monoclinic phases show that the ground states of the three compounds are monoclinic, although the energy difference between the monoclinic and tetragonal structures is very small in the case of Sr_2MgWO_6. The symmetry analysis of the distortions involved in the experimental and calculated low-temperature structures shows that the amplitude of two primary distortions associated to rigid rotations of the MX_6 and WO_6 octahedra are dominant, although the amplitude of a third mode related to deformations of the MX_6 groups can not be neglected. The energy maps of the space spanned by the three relevant modes are calculated, and the couplings among the modes are evaluated, showing that the role of a hard secondary mode (in the Landau sense) coupled trilinearly to the two primary instabilities is crucial to stabilize the monoclinic ground state. Results suggest that the key role of the trilinear coupling among three modes could be rather common. A phenomenological theory including the effects of the chemical pressure is also developed. We find that the evolution of the stiffness constants in terms of the atomic substitution follows an accurate linear dependence and that the influence of quantum saturation of the order parameters could stabilize the tetragonal phase of Sr_2MgWO_6.

DOI: 10.1103/PhysRevB.89.064107 PACS number(s): 61.50.Ks, 63.20.Ry, 31.15.A−, 64.70.K−

I. INTRODUCTION

Several decades of in-depth research have not been enough to reduce the interest in perovskite oxides. On the contrary, new theoretical challenges arise and the potential impact of new technological applications is explored intensively. Both theoretical and practical interests make the study of these materials extremely active nowadays. The ideal cubic ($Pm\bar{3}m$, No. 225) structure of the simple ABX_3 perovskites can be described in terms of a single variable: the lattice parameter a_p. However, the usual structure of perovskites is a more complex low-symmetry modification and must be described as a distorted structure with respect to the ideal cubic prototype. By far the most common distortion consists of rigid-unit modes (RUMs), in which the BX_6 octahedral units remain almost rigid and the rotations of the corner-linked units generate an antiferrodistortive distortion. The second type of distortion is ferroelectric, in which the A or B cations are displaced with respect to the rigid oxygen octahedra. The third type of distortion involves deformation of the X_6 octahedral units, being the amplitude of the associated displacements very small. Nevertheless, ferroelectric and antiferrodistortive distortions are not usually present in the same structure because the condensation of one mode inhibits the condensation of the other one due to a positive and strong biquadratic coupling. $BaTiO_3$, $KNbO_3$, or $PbTiO_3$ are typical examples of this behavior: the cubic phase is unstable with respect to both types of distortions [1,2], but once the ferroelectric mode condensates the structures are stable down to low temperatures.

More intricate scenarios appear in complex perovskite structures, where several distortions are needed to explain the symmetry lowering. Recent studies [3] show that ferroelectricity can be active in a scenario where the trilinear coupling of three modes, two rotational and one ferroelectric, plays a fundamental role. Similar mechanisms have been found in proper ferroelectrics such as the Aurivillius compound $SrBi_2Ta_2O_9$ (SBT) [4], improper ferroelectrics such as the Ruddlesden-Popper $Ca_2Mn_2O_7$ [5], the double perovskite $NaLaMnWO_6$ [6], and $PbTiO_3/SrTiO_3$ superlattices [7]. This trilinear coupling could also be responsible for the "avalanche" phase transitions, where several modes condense simultaneously [8,9] and could give a key in the field of material engineering in order to design new compounds with the appropriate properties [3,5,7,10].

The double perovskites Sr_2MWO_6 (M = Zn, Ca, Mg), subject of this work, do not present ferroelectricity, but the structure of the ground state, expressed as a distortion of the high-temperature cubic phase, allows the existence of a trilinear coupling among unstable modes that transform according to different irreducible representations. The same physical mechanism, the stabilization of the ground state through the coupling of three modes, could be active in these materials, and the evaluation of its role is a reasonable test to extend its applicability and confirm the relevance of the trilinear coupling whenever the phase transition involves the condensation of several modes.

II. EXPERIMENTAL STRUCTURES, PHASE TRANSITIONS, AND SYMMETRY ANALYSIS

The high-temperature structure of Sr_2MWO_6 (M = Ca, Cd, Mn, Zn, Co, Mg, and Ni) double perovskites is cubic with space group $Fm\bar{3}m$ (No. 225). At lower temperatures, they are tetragonal $I4/m$ (No. 87) and most of them (M = Ca, Cd, Mn, Zn, and Co) undergo another phase transition to a monoclinic structure with space group ($P2_1/n$, No.14, nonstandard setting) [11–15]. The intermediate tetragonal

*inigo.etxebarria@ehu.es

phase of the Mg and Ni double perovskites is stable down to the lowest temperatures [13,14]. The range of stability of the three phases is related to the size of the M cation: the larger the M cation, the higher all the transition temperatures and the narrower the stability of the tetragonal phase. For smaller M cations, the temperatures of the two phase transitions decrease, the range of stability of the tetragonal phase increases, and the monoclinic phase is stable in a narrower interval until it disappears. The three compounds studied in this work are representatives of the complete behavior of the family. In the Ca compound, the range of stability of the monoclinic phase is very wide (0–1150 K) and the tetragonal structure appears only in a very small temperature range between 1150 and 1250 K. The intermediate case corresponds to the Zn compound, where the tetragonal phase is stable between 340 and 770 K with a much narrower monoclinic phase (0–340 K). In the case of the Mg compound, the monoclinic phase has not been reported and the tetragonal phase remains stable from 570 down to 26 K [13].

Tetragonal ($I4/m$) and monoclinic ($P2_1/n$) space groups are subgroups of the parent $Fm\bar{3}m$ cubic phase, but there is no group-subgroup relation between both. In consequence, and according to Landau theory, the cubic-to-tetragonal transition can be continuous, but the tetragonal-to-monoclinic phase transition must have a first-order character. The group-subgroup relation of the monoclinic and tetragonal space groups with respect to the cubic space group allows the description of the intermediate- and low-temperature phases as distortions of the parent cubic structure. With the aid of AMPLIMODES (www.cryst.ehu.es) [16], the distorted structures can be expressed in terms of symmetry-adapted modes, and a hierarchy can be established among them according to their amplitudes. Table I shows the amplitudes of the two symmetry-adapted distortions that break the cubic symmetry, being compatible with the tetragonal intermediate phase. The isotropy subgroup of the Γ_4^+ irreducible representation is $I4/m$ and its amplitude is much larger than the other distortion, indicating that it corresponds to the primary order parameter of the cubic-to-tetragonal phase transitions, the Γ_3^+ distortion being a secondary effect. A similar symmetry analysis of the monoclinic structures is shown in Table II. The irreducible representations Γ_4^+ and Γ_3^+ are the same as in Table I, but due to the different directions of the Γ_4^+ irreps [(0,0,a) and (0,a,a)], the associated distortions are different. In order to avoid confusion, we will denote by Γ_{4T}^+ and Γ_{4M}^+ the tetragonal and monoclinic distortions, respectively. Although there is no experimental evidence of the existence of the monoclinic low-temperature structure of Sr_2MgWO_6, it is included in the table because, as it will be explained in the next section, according to calculations the structure of its ground state is monoclinic. Table II shows that the amplitudes of the Γ_4^+ and X_3^+ distortions are dominant. The isotropy subgroups of Γ_4^+ and X_3^+ are $C2/m$ and $P4/mnc$, respectively; as the intersection of these two groups is the observed $P2_1/n$ symmetry, the presence of these two distortion modes is sufficient to lower the symmetry from $Fm\bar{3}m$ to the one of the monoclinic phase, and both can be considered primary order parameters. The amplitude of the X_5^+ is not negligible, this distortion does not break the symmetry further, and it should be considered as a secondary order parameter coupled to the primary ones.

As usual in perovskites, the deformation of the MO_6 and WO_6 octahedra is small and the dominant distortions can be described by rigid unit modes (RUMs). The Γ_{4T}^+ mode involves rotations of the corner-linked octahedra with respect to the z axis, with antiphase rotation of successive octahedra along the axis [Fig. 1(a)]. It corresponds to the $a^0a^0c^-$ rotation according to the Glazer notation [17,18] and it is analogous to the R_4^+ mode of the simple perovskites [19,20]. The Γ_{4M}^+ distortion presents a similar scheme with the octahedra rotating around the (1,1,0) axis; it is shown in Fig. 1(b) and corresponds to $a^0b^-b^-$ tilts. The X_3^+ mode is related to the M_3^+ representation of the simple perovskites [19,20] and is composed by in-phase rotations of successive octahedra along the z axis ($a^+b^0b^0$) as shown in Fig. 1(c) [17,18]. Finally, the secondary X_5^+ distortion is not a RUM. The WO_6 octahedra remain almost rigid, they rotate around the (1,1,0) axis, and consecutive octahedra along the axis rotate in phase. However, the closest WO_6 octahedra in the plane perpendicular to the axis rotate in antiphase and, as a consequence, the MO_6 octahedra are distorted and can

TABLE I. Summary of the mode decomposition with respect to the $Fm\bar{3}m$ parent phase of the experimental and calculated $I4/m$ structures. In the three cases, the a_c parameter of the cubic structure is the same used in the calculations. There are not experimental data for the tetragonal structure of Sr_2CaWO_6.

			Amplitude (Å)				
		Isotropy	Ca	Zn		Mg	
Irrep	Direction	subgroup	Calc.	Expt.	Calc.	Expt.	Calc.
Γ_4^+	(0,0,a)	$I4/m$	1.04	0.71	0.72	0.48	0.61
Γ_3^+	(a,0)	$I4/mmm$	0.06	0.06	0.03	0.04	0.02

TABLE II. Summary of the mode decomposition with respect to the $Fm\bar{3}m$ parent phase of the experimental and calculated $P2_1/n$ structures in order of decreasing amplitudes. The X_5^+ and Γ_5^+ distortions involve several degrees of freedom; in these cases, the scalar product of the normalized experimental and calculated polarization vectors are given in parentheses. Although *ab initio* calculations give a stable monoclinic structure, there is not experimental evidence of the existence of such a phase for Sr_2MgWO_6.

			Amplitude (Å)				
		Isotropy	Ca		Zn		Mg
Irrep	Direction	subgroup	Expt.	Calc.	Expt.	Calc.	Calc.
Γ_4^+	(a,a,0)	$C2/m$	1.37	1.46	0.75	0.97	0.84
X_3^+	(0,a,0)	$P4/mnc$	0.95	0.98	0.40	0.64	0.49
X_5^+	(a,a,0,0,a,$-a$)	$Pnnm$	0.52	0.58	0.15	0.28	0.19
			(0.99)		(0.82)		
Γ_5^+	($-b$,a,$-a$)	$C2/m$	0.24	0.12	0.07	0.05	0.04
			(0.57)		(0.74)		
X_2^+	(0,a,0)	$P4_2/mnm$	0.05	0.02	0.06	0.00	0.00
Γ_3^+	(a,0)	$I4/mmm$	0.00	0.01	0.03	0.00	0.00

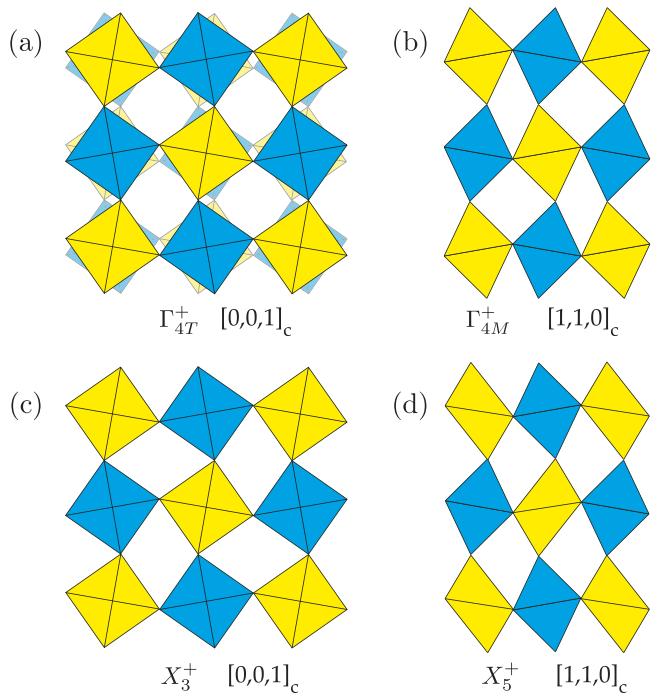

FIG. 1. (Color online) Schematic view in different projections with respect to the cubic axes of the rotations and slight deformations of the octahedral groups (WO_6 in blue and ZnO_6 in yellow) associated to the dominant distortions: (a) projection along the $[0, 0,1]_c$ direction of the Γ^+_{4T} RUM, (b) $[1, 1,0]_c$ projection of the Γ^+_{4M}, (c) $[0, 0,1]_c$ projection of the X^+_3 RUM, and (d) $[1, 1,0]_c$ projection of the X^+_5 distortion, where the WO_6 units remain rigid but the ZnO_6 octahedra are distorted. The magnitude of the distortions has been exaggerated for clarity.

not be considered rigid bodies [Fig. 1(d)]. These rotations are accompanied by displacements of the Sr ions in the xy plane.

III. COMPUTATIONAL DETAILS

The structures of the three compounds were relaxed by *ab initio* calculations to study the energy landscape in the space of the relevant distortions. Calculations were done for the cubic, tetragonal, and monoclinic structures using the WIEN2K code, based on the full-potential (L)APW+lo method. Exchange and correlation effects were treated within the GGA approximation with the Perdew-Burke-Ernzerhof parametrization. The radii of the atomic spheres were chosen as 1.86 (W), 2.02 (Zn), 2.29 (Sr), and 1.65 (O) bohrs for Sr_2ZnWO_6, 1.91 (W), 1.95 (Ca), 2.15 (Sr), and 1.69 (O) bohrs for Sr_2CaWO_6, and 1.90 (W), 1.89 (Mg), 2.18 (Sr), and 1.68 (O) bohrs in the case of Sr_2MgWO_6. The $R_{\rm mt}K_{\rm max}$ parameter was chosen to be 7.5 for all the compounds and calculations. A Monkhorst-Pack **k**-mesh of $4 \times 6 \times 4$ was used for the monoclinic calculations, which represents 24 independent **k** points in the irreducible Brillouin zone. In order to maintain the **k**-point density for all the calculations as constant as possible, a **k**-mesh of $7 \times 7 \times 7$ was used for the tetragonal and cubic cells. The choice of the parameters was preceded by energy difference convergence tests which confirmed their validity. The self-consistency convergence criterion was typically 0.0001 Ry for energy and 0.01 mRy/bohr for forces. In order to calculate the energies of distorted structures, force minimization calculations for all three compounds were performed at monoclinic, tetragonal, and cubic symmetries. Cubic and tetragonal structures accepted a high accuracy, of the order of 0.01 mRy/bohr. For relaxation of the monoclinic structure, forces below 0.4 mRy/bohr were obtained for $M =$ Zn and Mg. The highest force was below 0.7 mRy/bohr in the Ca compound. The influence of strain was neglected and the volume of the cell was fixed in all the calculations. If $\mathbf{a_c}$, $\mathbf{b_c}$, and $\mathbf{c_c}$ ($|\mathbf{a_c}| = |\mathbf{b_c}| = |\mathbf{c_c}| = a_c$) are the lattice vectors of the cubic structure, the tetragonal and monoclinic lattice vectors were fixed to $\mathbf{a_t} = \mathbf{a_m} = (\mathbf{a_c} - \mathbf{b_c})/2$, $\mathbf{b_t} = \mathbf{b_m} = (\mathbf{b_c} + \mathbf{a_c})/2$, and $\mathbf{c_t} = \mathbf{c_m} = \mathbf{c_c}$. Therefore, the density of each compound remains constant for the different symmetries. The a_c lattice parameter was chosen to reproduce the experimental density at the lowest temperature measured, monoclinic phase for Sr_2CaWO_6 and Sr_2ZnWO_6, and tetragonal phase for Sr_2MgWO_6 [13,14], giving $a_c = 8.2076$ Å, 7.9382 Å, and 7.9088 Å for the Ca, Zn, and Mg compounds, respectively.

IV. RESULTS

First, the relaxed structure under cubic symmetry was obtained for the three compounds to provide a reference that allows the analysis of the symmetry-breaking distortions. Then, the structures were relaxed under tetragonal symmetry. Tables I and III show the analysis of the symmetry-breaking distortions and the depth of the energy well of the tetragonal phase with respect to the cubic one. For the Zn and Mg compounds, the calculated and experimental amplitudes are similar, showing the very secondary role of the Γ^+_3 distortion. The calculated amplitudes of the Γ^+_4 mode for the Ca compound (there is no experimental structure determination) show the same trend with a significantly larger Γ^+_4 distortion. As expected, the higher the tetragonal-to-cubic transition temperature, the larger the amplitude and depth of the tetragonal energy well. As can be seen in Table III, the energy difference between the cubic and tetragonal structures is mainly due to the primary distortion, and the Γ^+_3 mode plays a very secondary role.

TABLE III. Depths of the energy wells per formula unit (in mRy) of several distortions with respect to the cubic phase: tetragonal phase with all the symmetry-allowed distortions included (Abs. tetra.), Γ^+_{4T} distortion alone, monoclinic phase with all the possible symmetry-allowed included (Abs. mono.), Γ^+_{4M} distortion alone and X^+_3 distortion alone.

	Ca	Zn	Mg
Abs. tetra.	42.0	13.0	6.7
Γ^+_{4T}	34.4	11.0	6.0
Abs. mono.	60.5	16.1	7.8
Γ^+_{4M}	38.9	11.8	6.7
X^+_3	30.0	7.5	3.3

TABLE IV. Calculated (first row) and experimental (second row) atomic positions of the monoclinic structures in relative units for M = Zn, Ca, and Mg. The W atoms are fixed by symmetry at the (0, 0, 0) positions and the Ca, Zn, and Mg atoms at (0, 0, 0.5). For the Sr_2MgWO_6, only the calculated values are shown.

	x	y	z
M = Ca			
Sr	0.009	0.541	0.248
	0.009	0.537	0.249
O1	− 0.087	− 0.027	0.227
	− 0.071	− 0.025	0.222
O2	0.269	− 0.189	0.043
	0.262	− 0.177	0.046
O3	0.183	0.272	0.049
	0.185	0.263	0.050
M = Zn			
Sr	0.004	0.523	0.249
	0.002	0.508	0.250
O1	− 0.060	− 0.009	0.239
	− 0.045	− 0.008	0.236
O2	0.267	− 0.212	0.030
	0.251	− 0.220	0.021
O3	0.210	0.269	0.031
	0.220	0.261	0.028
M = Mg			
Sr	0.003	0.516	0.250
O1	− 0.052	− 0.006	0.241
O2	0.263	− 0.220	0.027
O3	0.219	0.264	0.027

Table II shows the amplitudes of the distortions obtained from similar calculations in the monoclinic phases. The X_5^+ and Γ_5^+ distortions include three and four degrees of freedom, respectively, and the amplitude alone is not enough to give a complete description of the modes. For these distortions, the scalar product of the normalized experimental and calculated polarization vectors are also given. The hierarchy of the amplitudes is correctly reproduced being the calculated values systematically larger since they correspond to the 0-K structure. As usual, the worst agreement corresponds to the distortions with small amplitudes that do not contribute significantly to the description of the low-temperature phase. The comparison between the experimental and calculated structures is shown in Table IV, and the agreement in the case of the Ca and Mg compounds is extremely good. Sr_2MgWO_6 is tetragonal at 29 K and, although there is no experimental evidence for the existence of a monoclinic low-temperature phase, the present calculations give a $P2_1/n$ structure which lowers the energy of the tetragonal phase. Energies for different amplitudes of the dominant distortions with respect to the relaxed cubic phase are plotted in Fig. 2. The three compounds show the same general behavior: Γ_{4M}^+ and X_3^+ distortions are unstable while X_5^+ is hard. This fact reinforces the picture that the X_5^+ distortion plays a secondary role and becomes active through the coupling with the two primary order parameters. The scenario is very similar to that of $SrBi_2Ta_2O_9$ (SBT) [4] and $Ca_3Mn_2O_7$ [5], where a hard secondary mode becomes

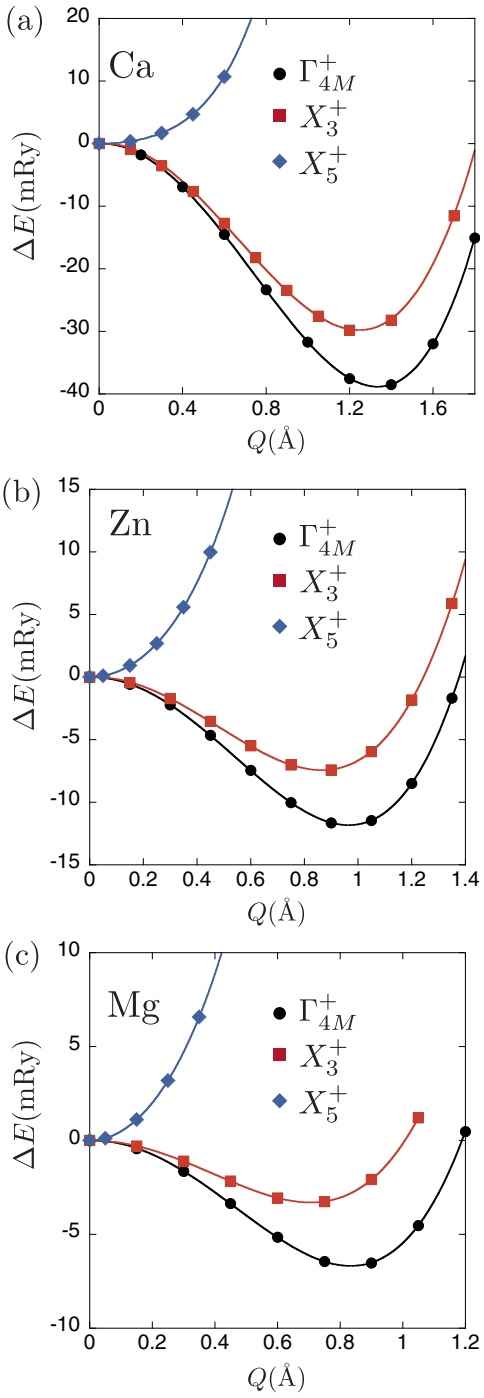

FIG. 2. (Color online) Energy per formula unit relative to the cubic relaxed structure in terms of the amplitudes (Q) of the Γ_{4M}^+, X_3^+, and X_5^+ distortions for the three compounds.

spontaneous due to a trilinear coupling with other two relevant modes. The depths of the energy wells are shown in Table III. The energy differences between the tetragonal and monoclinic phases are 18.8 (Ca), 3.3 (Zn), and 1.0 (Mg) mRy per formula unit. The tiny energy gain of the monoclinic phase of the Mg compound with respect to the tetragonal configuration and, as will be shown later, quantum fluctuations may be responsible for the stabilization of the tetragonal phase at low temperatures, and even at 0 K due to zero-point fluctuations. Nevertheless,

although the experimental strain is small for the Mg compound, it can not be discarded that optimization of the lattice constants for each symmetry could give a different phase stability.

The energies of the frozen pure-symmetry modes shown in Fig. 2 give an incomplete description as they are restricted to special directions of the energy map in the three-dimensional space spanned by the relevant modes. The energy of a general distortion and the quantification of the couplings among the modes can be studied by determining the polynomial that describes the energy variations around the cubic configuration in terms of the amplitudes of Γ_{4M}^+, X_3^+, and X_5^+ distortions. The energy difference between the cubic reference and the distorted structures can be expressed up to fourth order by

$$\Delta E\left(Q_{\Gamma_4^+}, Q_{X_3^+}, Q_{X_5^+}\right) = E_{\Gamma_4^+} + E_{X_3^+} + E_{X_5^+} + E_{\Gamma_4^+ X_3^+} + E_{\Gamma_4^+ X_5^+} + E_{X_3^+ X_5^+} + E_{\Gamma_4^+ X_3^+ X_5^+}.$$

The energy for the pure modes depicted in Fig. 2 is given by

$$E_{\Gamma_4^+} = \tfrac{1}{2}\kappa_{\Gamma_4^+} Q_{\Gamma_4^+}^2 + \beta_{\Gamma_4^+} Q_{\Gamma_4^+}^4,$$
$$E_{X_3^+} = \tfrac{1}{2}\kappa_{X_3^+} Q_{X_3^+}^2 + \beta_{X_3^+} Q_{X_3^+}^4,$$
$$E_{X_5^+} = \tfrac{1}{2}\kappa_{X_5^+} Q_{X_5^+}^2 + \beta_{X_5^+} Q_{X_5^+}^4.$$

The pair interactions are

$$E_{\Gamma_4^+ X_3^+} = \delta_{\Gamma_4^+ X_3^+} Q_{\Gamma_4^+}^2 Q_{X_3^+}^2,$$
$$E_{\Gamma_4^+ X_5^+} = \delta_{\Gamma_4^+ X_5^+} Q_{\Gamma_4^+}^2 Q_{X_5^+}^2,$$
$$E_{X_3^+ X_5^+} = \delta_{X_3^+ X_5^+} Q_{X_3^+}^2 Q_{X_5^+}^2$$

and the symmetry-allowed trilinear coupling is

$$E_{\Gamma_4^+ X_3^+ X_5^+} = t_{\Gamma_4^+ X_3^+ X_5^+} Q_{\Gamma_4^+} Q_{X_3^+} Q_{X_5^+}.$$

The polynomial coefficients have been determined by least-squares fits of the energies of more that 60 configurations for each compound obtained by *ab initio* calculations with different sets of amplitudes for the three distortions. The inclusion of sixth-order terms in the energy expansion did not provide a significant improvement in the fit and, in consequence, they have not been considered in the model. Table V shows the values of the coefficients that can be used to explore the energy landscape at any direction and any section to obtain more detailed information about the role that each mode plays in the phase transition.

TABLE V. Polynomial coefficients of the energy expansion obtained by least-squares fits for M = Ca, Zn, and Mg.

	Ca	Zn	Mg
$\kappa_{\Gamma_{4M}^+}$ (mRy/bohr^2)	− 23.59	− 13.95	− 10.17
$\kappa_{X_3^+}$ (mRy/bohr^2)	− 19.48	− 10.60	− 7.19
$\kappa_{X_5^+}$ (mRy/bohr^2)	6.72	21.91	26.56
$\beta_{\Gamma_{4M}^+}$ (mRy/bohr^4)	0.89	1.03	1.00
$\beta_{X_3^+}$ (mRy/bohr^4)	0.80	0.95	0.99
$\beta_{X_5^+}$ (mRy/bohr^4)	3.75	3.85	3.84
$\delta_{\Gamma_{4M}^+ X_3^+}$ (mRy/bohr^4)	1.58	1.82	1.81
$\delta_{\Gamma_{4M}^+ X_5^+}$ (mRy/bohr^4)	0.49	0.50	0.54
$\delta_{X_3^+ X_5^+}$ (mRy/bohr^4)	1.07	0.91	1.09
$t_{\Gamma_{4M}^+ X_3^+ X_5^+}$ (mRy/bohr^3)	− 7.12	− 7.48	− 7.94

The monoclinic ground state corresponds to a mixed configuration with the three modes frozen, but, as stated above, the presence of two main order parameters Γ_{4M}^+ and X_3^+ is enough to break the symmetry to the observed one. Figure 3(a) shows the energy of the X_3^+ mode alone, and with the amplitude of Γ_{4M}^+ distortion fixed to 1.0 Å for the Zn compound. The presence of the nonzero Γ_{4M}^+ distortion stabilizes the X_3^+ configuration due to the strong positive biquadratic coupling $\delta_{\Gamma_{4M}^+ X_3^+}$. Figure 4(a) shows the energy contour map of the $(Q_{\Gamma_{4M}^+}, Q_{X_3^+})$ section for the Ca compound, and again, the biquadratic coupling penalizes the freezing of the two main modes simultaneously as usual [4,8]. In addition, the minimum

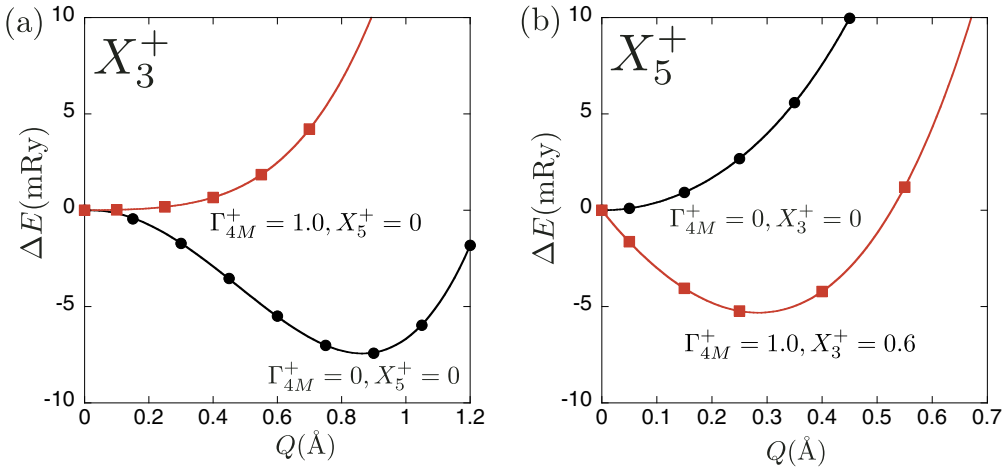

FIG. 3. (Color online) (a) Energy of the Zn compound as a function of the amplitude of the pure X_3^+ mode (squares), and with the amplitude of the Γ_{4M}^+ distortion fixed to 1 Å (circles). (b) Energy of the Zn compound in terms of the amplitude of the pure secondary X_5^+ mode (circles), and with the amplitude of the Γ_{4M}^+ and X_3^+ distortions fixed to 1 and 0.6 Å, respectively (squares). The pure X_5^+ mode is hard but it becomes unstable when the other two distortions are switched on due to the trilinear coupling. The plots have been shifted vertically to fix a common origin.

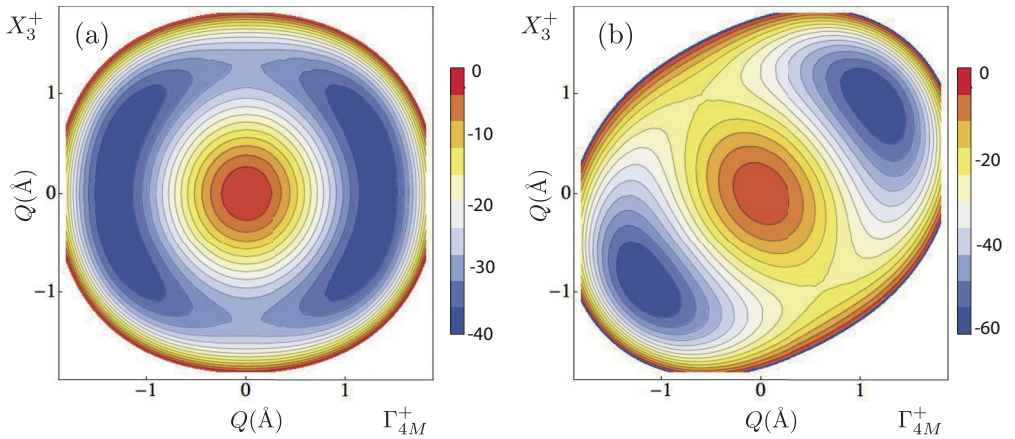

FIG. 4. (Color online) (a) Energy contour map of the $(Q_{\Gamma_{4M}^+}, Q_{X_3^+})$ section for the Ca compound with $Q_{X_5^+} = 0.0$. The minimum corresponds to the pure $Q_{\Gamma_{4M}^+}$ mode. (b) The same section with $Q_{X_5^+} = 0.6$ Å. The minimum corresponds to the experimentally observed mixed configuration. The units of the color bars are mRy per formula unit.

energy in this section is found at $Q_{\Gamma_{4M}^+} \approx 1.3, Q_{X_3^+} = Q_{X_5^+} = 0$ which corresponds to the $C2/m$ space group.

The inclusion of the X_5^+ distortion is essential to explain the stability of the experimental ground state. Figure 3(b) corresponds to the Zn compound, and it shows the energy versus the amplitude of the $Q_{X_5^+}$ mode alone, and with a mixed Γ_{4M}^+, X_3^+ distortion with amplitudes 1.0 and 0.6 Å, respectively. The hard X_5^+ pure distortion becomes unstable when the other two modes condense. The strong trilinear coupling, independently of its sign, is the critical ingredient to stabilize the monoclinic phase. In Fig. 4(b), the $(Q_{\Gamma_{4M}^+}, Q_{X_3^+})$ section of the Ca compound is plotted when the X_5^+ mode is frozen with an amplitude of 0.6 Å, and the absolute minimum which corresponds to a mixed configuration is clearly observed. The same general trend is observed for the three compounds, and the scenario is very similar to that of SBT [4] and Ca_2MnO_7 [5] where the role of an apparently secondary symmetry mode becomes critical to explain the existence and symmetry of the ground state.

V. PHASE DIAGRAM

A detailed analysis of the numerical values in Table V reveals that, apart from the second-order terms, the values of the rest of the coefficients, including the trilinear coupling, are very similar for the three compounds. As shown above, the trilinear terms stabilize the ground states, but the differences in the range of stability of the cubic, tetragonal, and monoclinic phases are governed almost exclusively by the stiffness constants (κ).

The calculated polynomial expansions of the energies can be considered as free energies at 0 K and, according to Landau theory, the free energies at finite temperatures can be approximated by taking into account the renormalization of the quadratic terms by thermal effects. In first approximation, the stiffness constants follow a linear law $\kappa(T) = a(T - T_0)$ and the rest of coefficients can be considered constant. Figure 5 shows the stability ranges of the different phases of Sr_2ZnWO_6 in terms of the stiffness constants of the two unstable modes: $\kappa_{\Gamma_{4M}^+}$ and $\kappa_{X_3^+}$. The $\kappa_{X_5^+}$ coefficient has been assumed to vary in such a way that its difference with the $\kappa_{X_3^+}$ stiffness remains constant. The arrow corresponds to the path that crosses the ground state of Sr_2ZnWO_6 with a homogeneous renormalization of the stiffness constants of the three modes. The fact that Ca and Mg compounds lie on the same path indicates a linear relation among the stiffness constants of the three compounds. As the radius of the M cation decreases

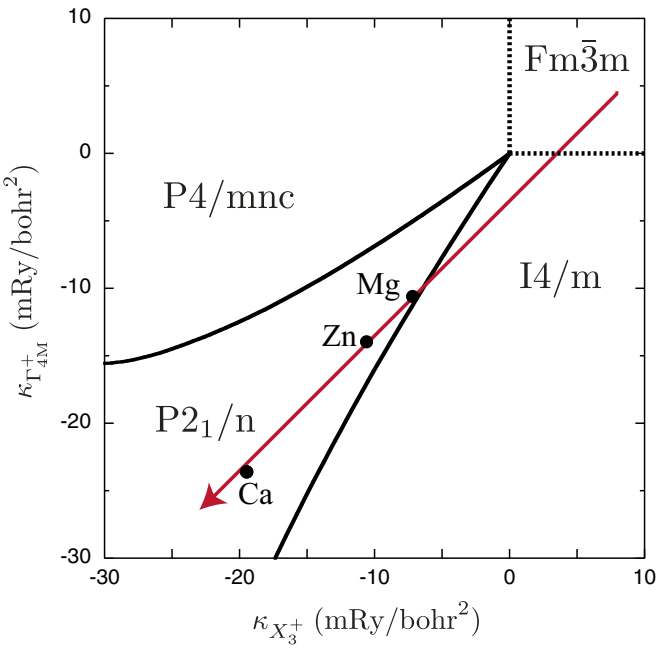

FIG. 5. (Color online) Phase diagram according to the polynomial expansion of Sr_2ZnWO_6 but with varying values of the quadratic coefficients $\kappa_{\Gamma_{4M}^+}$ and $\kappa_{X_3^+}$. The dotted lines are second-order phase transitions and the solid lines first order. The arrow shows a hypothetical path along which the renormalization of the three stiffness constants is homogeneous and passes through the ground state of Sr_2ZnWO_6. The location of the ground states of the other two compounds is also shown.

from Ca to Zn and Mg, the stiffness constants of the three modes increase and this hardening of the three modes seems to be responsible for the main features of the phase diagram in terms of temperature and radius of the M cations [12]. The change in volume of the M cation corresponds to a chemical pressure (z) that in the lowest order is coupled to the order parameter as $\propto zQ^2$ and produces a renormalization of the quadratic coefficients similar to the thermal renormalization [22]. Both thermal and pressure renormalization can be taken into account by the following quadratic terms in the free energy:

$$\begin{aligned}\Delta F = &\frac{a_{\Gamma_4^+}}{2}(T - T_{0,\Gamma_4^+} + k_{\Gamma_4^+} z)Q^2_{\Gamma_4^+} \\ &+ \frac{a_{X_3^+}}{2}(T - T_{0,X_3} + k_{X_3^+} z)Q^2_{X_3^+} \\ &+ \frac{a_{X_5^+}}{2}(T - T_{0,X_5} + k_{X_5^+} z)Q^2_{X_5^+}. \qquad (1)\end{aligned}$$

By fixing the origin and rescaling the chemical pressure, we have chosen $z_{\mathrm{Ca}} = 0$ and $z_{\mathrm{Mg}} = 1$ without loss of generality. We have used the nine values of the κ stiffness constants of Table V and the five known experimental transition temperatures to obtain the coefficients of the quadratic terms of the free energy and the value of z_{Zn} by a least-squares fitting. Results are shown in Table VI and Fig. 6. According to Fig. 6(a), the dependence of the stiffness constants with respect to the chemical pressure follows very faithfully the linear ansatz, and up to our knowledge this is the first quantitative verification of such a behavior by first-principles calculations. Although experimentally Sr_2MgWO_6 remains tetragonal at low temperatures, this model gives a tetragonal-to-monoclinic phase transition at $T = 157$ K [Fig. 6(b)].

Quantum effects can be included in this phenomenological approach by applying the following quantum correction to the quadratic terms [21–23]:

$$\frac{a'}{2}\theta\left(\coth\frac{\theta}{T} - \coth\frac{\theta}{T'_0} + \frac{k'}{\theta}z\right)Q^2, \qquad (2)$$

where the saturation temperature θ characterizes the temperature of the crossover between classical and quantum behavior. We have performed again a least-squares fit of the known data using the quantum model for the X_3^+ order parameter with a new constraint to force the tetragonal-to-monoclinic phase transitions to be at 0 K for the Mg compound. As listed in Table VI, z_{Zn} and the coefficients of the Γ_4^+ mode remain unchanged and the obtained value for the saturation temperature ($\theta_{X_3^+} = 170$ K) is comparable to the values found in the literature [22]. The dotted line of Fig. 6(b) shows that the classical and quantum phase diagrams are indistinguishable for low chemical pressures and that the quantum saturation of one of the modes is enough to suppress the low-temperature phase transition in the Sr_2MgWO_6 compound.

TABLE VI. a, T_0, and k: coefficients of the quadratic term of free energy according to the classic behavior of Eq. (1). The fitted value of the chemical pressure for the Zn compound is $z_{\mathrm{Zn}} = 0.706$. a', T'_0, and k': coefficients including the quantum correction for X_3^+ with $\theta_{X_3^+} = 170$K [Eq. (2)]; the coefficients for Γ_4^+ are the same in both cases.

	Γ_4^+	X_3^+	X_5^+
a (mRy bohr^{-2} K^{-1})	0.01856	0.01562	0.1264
T_0 (K)	1250	1244	−55
k (K)	680	790	159
a' (mRy bohr^{-2} K^{-1})	0.01856	0.01566	0.0942
T'_0 (K)	1250	1241	−74
k' (K)	680	788	214

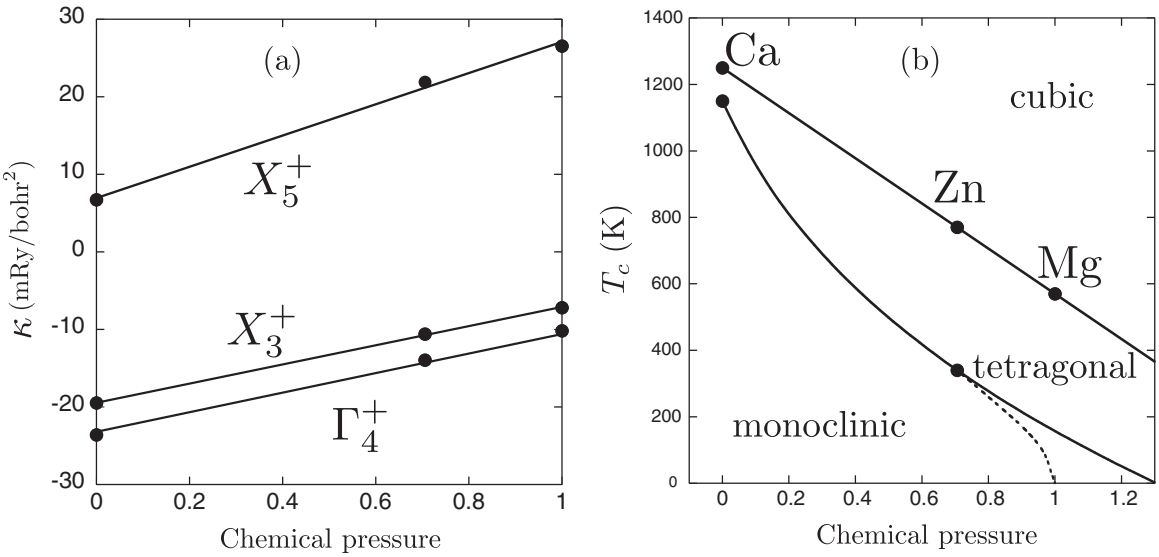

FIG. 6. (a) Linear behavior of the stiffness constants according to the least-squares fit with $z_{\mathrm{Zn}} = 0.705$. (b) Transition temperatures of the classic (solid line) model and and quantum correction (dotted line) with $\theta_{X_3^+} = 170$ K.

VI. CONCLUSIONS

First-principles calculations for the double perovskites Sr_2MWO_6 (M = Zn, Ca, Mg) show that the ground states of the three compounds are monoclinic ($P2_1/n$, No.14). Experiments report that the low-temperature phase of Sr_2MgWO_6 is tetragonal, however, present calculations show a small energy difference per formula unit of $\sim$1 mRy in favor of the monoclinic phase when the density of each compound remains constant for the different symmetries.

Symmetry analysis of the distortions involved in the experimental and calculated low-temperature structures shows the primary role of two distortions associated to RUMs of symmetry Γ^+_{4M} and X^+_3. Energy calculations show that the cubic reference structure is unstable with respect to the two primary distortions, but the strong biquadratic coupling inhibits the simultaneous condensation of both. A third distortion of symmetry X^+_5 associated to deformations of the MX_6 octahedra must be taken into account to justify the existence of a monoclinic ground state. Although the stiffness constant of the third mode is positive, a strong trilinear coupling among the three modes is the ultimate cause of the stabilization of the observed ground state. This mechanism has been already observed in several ferroelectrics, and present results suggest that the presence and relevance of a trilinear coupling could be almost universal when the symmetry breaking at the phase transition involves several modes.

A phenomenological approach in terms of the chemical pressure associated to the change of the radius of the M cation shows a very accurate linear behavior of the quadratic terms of the Landau expansion with respect to the chemical pressure, while higher-order terms remain essentially constant. Finally, the inclusion of quantum corrections in the model reveals that quantum effects can be responsible of the stabilization of the monoclinic phase in the case of Sr_2MgWO_6, solving the discrepancy with the experimental phase diagram.

ACKNOWLEDGMENTS

We gratefully thank J. M. Igartua and J. M. Perez-Mato for helpful discussions. This work has been supported by the Basque Government (Project No. IT-779-13) and the Spanish Ministry of Education and Science (Project No. MAT2012-34740). One of the authors (U.P.) gratefully acknowledges the financial support of the UPV/EHU. Computational resources were provided by the SGI/IZO-SGIker at the UPV/EHU.

[1] P. Ghosez, E. Cockayne, U. V. Waghmare, and K. M. Rabe, Phys. Rev. B **60**, 836 (1999).
[2] R. Yu and H. Krakauer, Phys. Rev. Lett. **74**, 4067 (1995).
[3] P. Ghosez and J. M. Triscone, Nat. Mater. **10**, 269 (2011).
[4] J. M. Perez-Mato, M. Aroyo, Alberto García, P. Blaha, K. Schwarz, J. Schweifer, and K. Parlinski, Phys. Rev. B **70**, 214111 (2004).
[5] N. A. Benedek and C. J. Fennie, Phys. Rev. Lett. **106**, 107204 (2011).
[6] T. Fukushima, A. Stroppa, S. Picozzi, and J. M. Perez-Mato, Phys. Chem. Chem. Phys. **13**, 12186 (2011).
[7] E. Bousquet, M. Dawber, N. Stuchi, C. Lichtensteiger, P. Hermet, S. Gariglio, J. M. Triscone, and P. Ghosez, Nature (London) **452**, 732 (2008).
[8] J. M. Perez-Mato, P. Blaha, K. Schwarz, M. Aroyo, D. Orobengoa, I. Etxebarria, and Alberto Garcia, Phys. Rev. B **77**, 184104 (2008).
[9] I. Etxebarria, J. M. Perez-Mato, and P. Boullay, Ferroelectrics **401**, 17 (2010).
[10] J. M. Rondinelli and C. J. Fennie, Adv. Mater. **24**, 1961 (2012).
[11] B. Manoun, J. M. Igartua, M. Gateshki, and S. K. Saxena, J. Phys.: Condens. Matter **16**, 8367 (2004).
[12] M. Gateshki, J. M. Igartua, and A. Faik, J. Solid State Chem. **180**, 2248 (2007).
[13] M. Gateshki, J. M. Igartua, and E. Hernández-Bocanegra, J. Phys.: Condens. Matter **15**, 6199 (2003).
[14] M. Gateshki and J. M. Igartua, J. Phys.: Condens. Matter **16**, 6639 (2004).
[15] A. Faik, J. M. I. Gartua, G. J. Cuello, F. Jimnez-Villacorta, G. R. Castro, and L. Lezama, J. Mol. Struct. **933**, 53 (2009).
[16] D. Orobengoa, C. Capillas, M. I. Aroyo, and J. M. Perez-Mato, J. Appl. Crystallogr. **42**, 820 (2009)
[17] A. M. Glazer, Acta Crystallogr., Sect. B: Struct. Crystallogr. Cryst. Chem. **28**, 3384 (1972).
[18] A. M. Glazer, Acta Crystallogr., Sect. A: Cryst. Phys., Diffr., Theor. Gen. Crystallogr. **31**, 756 (1975).
[19] C. J. Howard and H. T. Stokes, Acta. Crystallogr., Sect. B: Struct. Crystallogr. Cryst. Chem. **54**, 782 (1998).
[20] C. J. Howard, B. J. Kennedy, and P. M. Woodward, Acta. Crystallogr., Sect. B: Struct. Crystallogr. Cryst. Chem. **59**, 463 (2003).
[21] E. K. H. Salje, B. Wruck, and H. Thomas, Z. Phys. B: Condens. Matter **82**, 399 (1991).
[22] S. A. Hayward and E. K. H. Salje, J. Phys.: Condens. Matter **10**, 1421 (1998).
[23] J. M. Perez-Mato and E. K. H. Salje, J. Phys.: Condens. Matter **12**, L29 (2000).